Mueller matrix spectroscopic ellipsometry study of chiral nanocrystalline cellulose films

OPEN ACCESS
IOP Publishing
Journal of Optics
J. Opt. **20** (2018) 024001 (10pp)
https://doi.org/10.1088/2040-8986/aa9e7d

Mueller matrix spectroscopic ellipsometry study of chiral nanocrystalline cellulose films

Arturo Mendoza-Galván[1], Eloy Muñoz-Pineda[1], Sidney J L Ribeiro[2], Moliria V Santos[2,4], Kenneth Järrendahl[3,5] and Hans Arwin[3]

[1] Cinvestav-IPN, Unidad Querétaro, Libramiento Norponiente 2000, 76230 Querétaro, Mexico
[2] Institute of Chemistry São Paulo State University- UNESP, Araraquara SP, Brazil
[3] Materials Optics, Department of Physics, Chemistry and Biology, Linköping University, SE-581 83 Linköping, Sweden

E-mail: amendoza@cinvestav.mx, keloyito@hotmail.com, sidney@iq.unesp.br, moliria.santos@gmail.com, kenneth.jarrendahl@liu.se and hans.arwin@liu.se

Received 25 October 2017, revised 26 November 2017
Accepted for publication 30 November 2017
Published 4 January 2018

Abstract

Chiral nanocrystalline cellulose (NCC) free-standing films were prepared through slow evaporation of aqueous suspensions of cellulose nanocrystals in a nematic chiral liquid crystal phase. Mueller matrix (MM) spectroscopic ellipsometry is used to study the polarization and depolarization properties of the chiral films. In the reflection mode, the MM is similar to the matrices reported for the cuticle of some beetles reflecting near circular left-handed polarized light in the visible range. The polarization properties of light transmitted at normal incidence for different polarization states of incident light are discussed. By using a differential decomposition of the MM, the structural circular birefringence and dichroism of a NCC chiral film are evaluated.

Keywords: Mueller matrix, chiral films, biomimetic materials

(Some figures may appear in colour only in the online journal)

1. Introduction

Helicoidal structures of cellulose, chitin or collagen microfibrils are commonly found in nature [1, 2]. These helicoidal arrangements are often referred to as twisted lamellae (Bouligand) structures. Depending on rotation direction the helical structure is defined as right- or left-handed. The characteristic length to complete a rotation of 360° defines the helix *pitch* (Λ). In some plants, the helicoidal structure of cellulose microfibrils produces iridescent colors in leaves and fruits [3]. Some beetles exhibit circular polarization features and in some cases also with metallic shine due to chitin-protein fibrils arranged in parallel lamellae comprising a Bouligand structure in the exoskeleton (cuticle) [4]. Both for plants and beetles, unpolarized incident light is selectively reflected with the same handedness as the chiral structure producing the bright colors observed. This is due to the circular Bragg phenomenon commonly referred to as selective Bragg reflection [5]. At normal incidence, selective reflection takes place in a spectral band centered at wavelength $\lambda_0 = n_{av}\Lambda$, where n_{av} is the in-plane average refractive index. Thus, an analogy with the cholesteric (chiral nematic) phase of some liquid crystals is straightforward.

Since decades, natural helicoidal structures have inspired the development of processes for optical biomimetics leading to the discovery of the helicoidal self-ordering of cellulose microfibrils in aqueous suspensions [6]. At that time, slow evaporation of the suspensions produced chiral films with pitch of a few microns mimicking the left-handed helicoidal arrangement of natural systems. Over the years, the research

[4] Current address: São Carlos Institute of Physics, University of São Paulo, PO Box 369, 13560-970, São Carlos, SP, Brazil
[5] Author to whom any correspondence should be addressed.

on nanocrystalline cellulose (NCC) chiral films showing iridescent colors progressed and nowadays it is an intense field of research carried out by several groups around the world [7–16]. In those works, the effect of the diverse processing parameters on the microstructure and optical properties of the NCC chiral films have been investigated. The complexity of the process involves many physicochemical phenomena occurring during film formation. Among them, the competition between glass formation and liquid crystal self-assembly has been identified as a source of film inhomogeneity [9]. The lack of uniformity in the films produces a mosaic texture with domains in the micrometer scale. The optical performance of NCC chiral films has been studied by several groups by measuring the reflected or transmitted irradiance for unpolarized, right-and left-handed circularly polarized (LHCP) incident light, as well as characterization of their circular dichroism (CD) [7, 14, 15]. Although these techniques account for the selective Bragg reflection of near-circular polarized light, a more extensive study of the polarization and depolarization properties of light reflected or transmitted by NCC chiral films has not been performed yet. Recently, we have used variable angle Mueller-matrix spectroscopic ellipsometry for a complete characterization of light reflected from the cuticle of several species of beetles [17–22]. We have then used a multiple angle of incidence approach to account for the angular and spectral shift characteristic of these all-dielectric reflective systems. Moreover, the knowledge of the Mueller matrix of an optical system allows determination of the polarization and depolarization capabilities of the system for any polarization state of the incident beam. These capabilities have not been investigated for NCC chiral films and a comparison with those exhibited by the cuticle of beetles could offer an opportunity to explore possible optical applications.

In this work, we study the polarization and depolarization properties of NCC free-standing chiral films in reflection and transmission modes using Mueller-matrix spectroscopic ellipsometry. In section 2, the experimental details are described. In section 3.1, the properties of the Mueller matrix of NCC chiral films in reflection mode for oblique incidence are discussed and compared with those of beetle cuticle. Also, the polarization properties of light reflected for incident unpolarized light are determined. In section 3.2, the Mueller matrix of NCC chiral films in transmission mode at normal incidence is reported. The polarization properties of transmitted light for unpolarized and circularly polarized incident beams are determined in section 3.3. The case of linearly polarized incident light is discussed in section 3.4. In section 3.5, application of the differential decomposition of the transmission Mueller matrix measured at normal incidence is analyzed. In the last section, some concluding remarks are presented.

2. Experimental details

2.1. Sample preparation

Dried bacterial cellulose membranes were milled to pass through a 0.5 mm screen to ensure uniform particle size and to increase the surface area. The milled pulp was hydrolyzed in 8.75 ml of a sulfuric acid solution per gram of pulp at a concentration of 64 wt% at 50 °C for 0.5 h under vigorous stirring. The bacterial cellulose suspension was then diluted with cold water (10 times the volume of the acid solution) to stop the hydrolysis, and allowed to settle overnight. The clear top layer was decanted, and the remaining cloudy layer was centrifuged at 6000 rpm for 10 min (Jouan C3i-CR3i multifunction centrifuge). The supernatant was decanted, and the resulting thick white suspension was washed three times with water to remove water soluble cellulose materials. The thick white suspension was dialyzed against water for one to four days in cellulose membrane tubes (12 000–14 000 molecular weight cut-off). The suspension was diluted to the desired concentration and then dispersed by ultrasound treatment in a sonicator (Sonics Vibra-Cell VC 505 500 W 20 kHz) with a 6 mm diameter probe. Typically, 50 ml of a 3.0 wt% NCC suspension was placed in a 100 ml plastic tube and sonicated at 60% of the maximum power (300 W). Prolonged sonication (to an energy input of over 700 J g^{-1} of NCC) was performed in an ice bath to prevent desulfation caused by the suspension heating. The suspension (8 ml) was transferred to a polystyrene Petri dish (diameter of 45 mm) and allowed to evaporate under ambient conditions until yielding solid films with chiral nematic organization.

2.2. Basics of Mueller matrix

The most general description of the polarization and depolarization capabilities of a sample requires the use of Stokes vectors and Mueller matrices [23]. A Stokes vector has four components (I, Q, U, V) which are expressed in terms of the irradiances of six basic polarization states: I_p, I_s, $I_{+45°}$, and $I_{-45°}$ corresponding to linear polarization parallel (p), perpendicular (s), at +45° and at −45° relative to the plane of incidence, respectively; and the other two corresponding to right- and LHCP light I_R and I_L, respectively. The explicit form of the Stokes vectors is

$$\mathbf{S} = \begin{bmatrix} I \\ Q \\ U \\ V \end{bmatrix} = \begin{bmatrix} I_p + I_s \\ I_p - I_s \\ I_{+45°} - I_{-45°} \\ I_R - I_L \end{bmatrix}. \tag{1}$$

In the Mueller–Stokes description, the light-sample interaction is accounted for by a linear relationship between the Stokes vectors of incident ($\mathbf{S}_i$) and outgoing ($\mathbf{S}_o$) light beams, through a 4 × 4 Mueller matrix ($\mathbf{M}$),

$$\mathbf{S}_o = \mathbf{M}\mathbf{S}_i = \begin{bmatrix} m_{11} & m_{12} & m_{13} & m_{14} \\ m_{21} & m_{22} & m_{23} & m_{24} \\ m_{31} & m_{32} & m_{33} & m_{34} \\ m_{41} & m_{42} & m_{43} & m_{44} \end{bmatrix} \mathbf{S}_i. \tag{2}$$

In this work, normalized Mueller matrices ($m_{11} = 1$) and Stokes vectors $\mathbf{S}_i$ ($I_p + I_s = 1$) are used.

After interaction with the sample, the light beam (reflected or transmitted) in general will emerge partially

polarized with a degree of polarization P given by [23],

$$P = \frac{\sqrt{Q^2 + U^2 + V^2}}{I}. \quad (3)$$

The polarized component of the emerging beam in general will be elliptically polarized with ellipticity e [17],

$$e = \tan\left(\frac{1}{2}\arcsin\frac{V}{\sqrt{Q^2 + U^2 + V^2}}\right), \quad (4)$$

where $-1 \leqslant e \leqslant +1$. The extrema correspond to left- and right-handed circularly polarized (RHCP) light, respectively; for linearly polarized light, $e = 0$, and other values of e are for elliptical polarization. The major axis of the polarization ellipse is located at an azimuthal angle φ measured from the plane of incidence and is given by [23],

$$\varphi = \frac{1}{2}\arctan(U/Q). \quad (5)$$

2.3. Characterization techniques

The Mueller matrix measurements were performed with a dual rotating compensator ellipsometer (RC2, J. A. Woollam Co., Inc.) in the wavelength (λ) range 245–1000 nm. Since the films are inhomogeneous and not flat, focusing probes were used to achieve a beam spot with size below 100 μm. Images of the area measured were acquired with a CCD camera attached to the RC2 system. More details about the instrument can be found in [17–22]. Measurements in transmission mode were done at normal incidence whereas in reflection mode, measurements were performed at angles of incidence (θ) between 20° and 75° in steps of 5°. The transmitted irradiance of unpolarized light at normal incidence on areas of 2 mm in diameter was measured in the spectral range of 240–840 nm using a FilmTek 3000 system (SCI, Inc.). The transmittance of circular right- and left-handed polarized light was also measured using commercial plastic-sheets filters (Edmund Optics), which show good performance in the 400–700 nm wavelength range as evaluated with the RC2 system. The thickness of the film was determined from cross-section scanning electron microscopy (SEM) images using a JXA-8530F system (JEOL).

3. Results and discussion

3.1. Mueller matrix and polarization properties of NCC chiral films in reflection mode

The Mueller-matrix spectroscopic ellipsometry data of an NCC chiral film are shown as function of wavelength and angle of incidence in the contour map in figure 1(a). A careful inspection provides the following relationships for all angles of incidence: $m_{12} = m_{21}$, $m_{13} = -m_{31}$, $m_{14} = m_{41}$, $m_{23} = -m_{32}$, $m_{24} = m_{42}$, and $m_{34} = -m_{43}$. As was earlier reported for beetle cuticles [20], these symmetries in **M** result from the constraint for cross polarization coefficients in chiral systems $r_{ps} = -r_{sp}$. The band of selective reflection of left-handed polarized light is identified by the negative values of m_{41} (yellow–red regions). At $\theta = 20°$, this band is centered at 516 nm and shifts to shorter wavelengths at larger angles of incidence. It is known that at oblique incidence the wavelength of selective reflection is given by $\lambda_m = n_{av}\Lambda\cos\theta_t$, where θ_t is the angle of wave propagation inside the helicoidal structure determined from Snell's law $n_a \sin\theta = n_{av}\sin\theta_t$ [24]. Therefore, taking $n_a = 1$ and $n_{av} = 1.54$ [25] the corresponding pitch is 343 nm. At wavelengths outside the band of selective reflection, **M** shows a behavior typical for dielectric materials [20]. For comparison, the data of **M** from the cuticle of the beetle *C. mutabilis* [21] is shown in figure 1(b). It can be noticed the similarities between the contour maps in figure 1 which shows that the polarization and depolarization properties of NCC chiral films and beetle cuticles are qualitatively similar.

As was mentioned above, NCC chiral films are characterized by a mosaic-like texture as can be observed in the image on the left in figure 2. This texture identifies the multidomain type and is characterized by both, random helix direction and pitch length distribution. Single-domain structures are characterized by the presence of a single helical structure selectively reflecting a well-defined band of wavelengths. In the image of the NCC chiral film in figure 2, we can see domains of different colors (blue, green, red), which define it as the multidomain type. Therefore, measurements at different places show selective reflection bands with different spectral characteristics. On the other hand, the image on the right in figure 2 corresponds to the cuticle of the beetle *C. mutabilis* where a more uniform color is seen. From the latter observation, it can be tempting to assume that the cuticle of beetles is of the single-domain type. However, the cuticle of *C. mutabilis* is comprised of chiral layers of different pitch, being larger near the surface.

In order to be physically meaningful, any experimentally determined Mueller matrix must fulfill several requirements. Among others, the system must not over-polarize incident polarized light. In quantitative terms, this means that the depolarizance (D) given by [26],

$$D = 1 - \left|\left[\frac{1}{3}\left(\frac{\mathrm{tr}(\mathbf{M}^{\mathrm{T}}\mathbf{M})}{m_{11}^2} - 1\right)\right]^{1/2}\right|, \quad (6)$$

shall be in the range $0 \leqslant D \leqslant 1$. In equation (6), T and tr stand for transpose and trace, respectively and $m_{11} = 1$ in our case. Thus, D gives the average measure of the depolarization produced by a system for all incident pure states. For a pure depolarizer $D = 1$ and $D = 0$ for a non-depolarizing pure system. Figure 3 shows D of the NCC chiral film in a contour polar representation where the radial and angular coordinates correspond to the wavelength λ and angle of incidence θ, respectively. As can be noticed, $D \leqslant 1$ and **M** is thus not over-polarizing. The largest values of D are found in the band of selective reflection, which is similar to the observation in the data measured on the cuticle of beetles [20, 21]. However, NCC chiral films are more depolarizing than beetle cuticle.

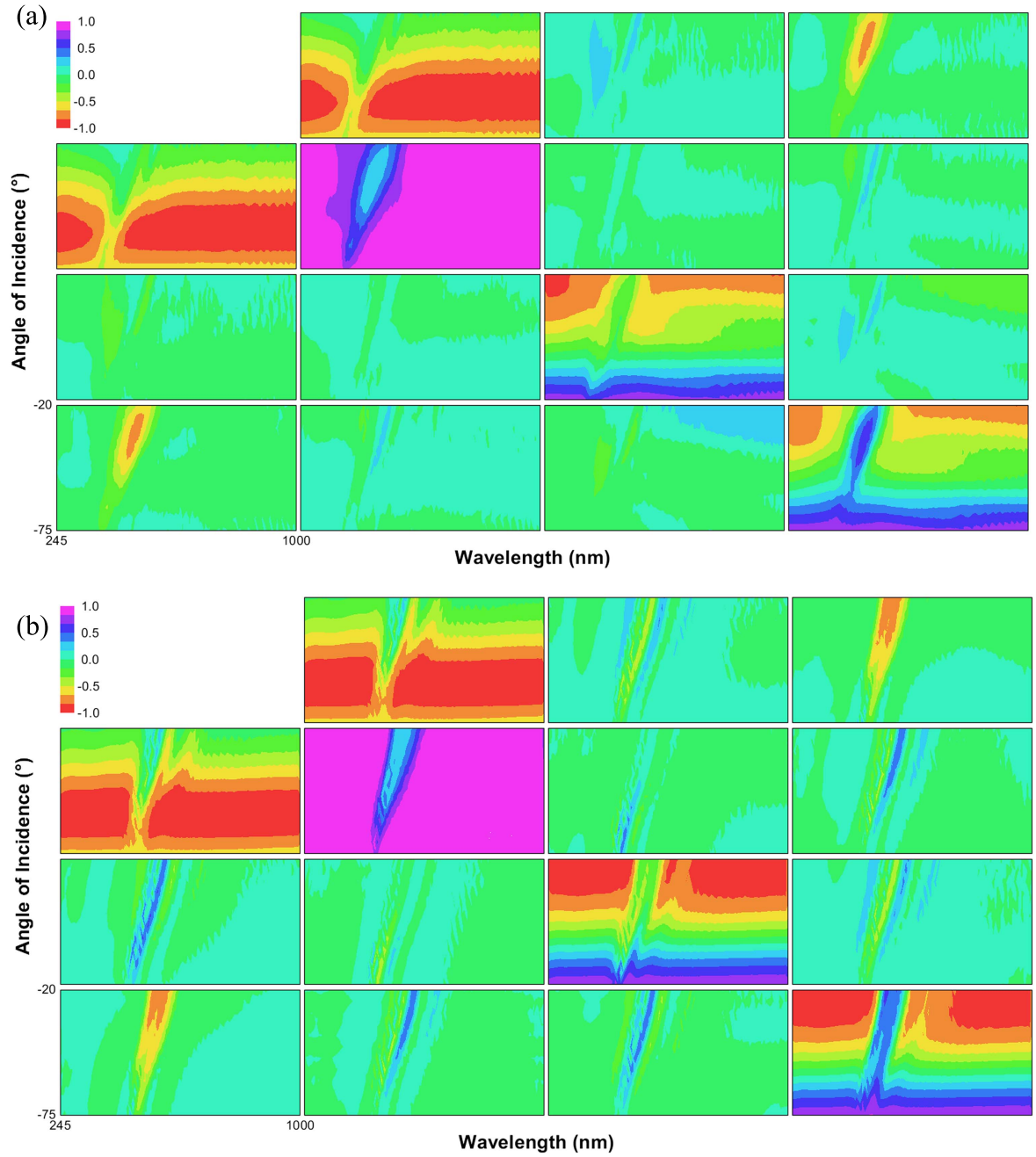

Figure 1. Contour maps of Mueller matrices in reflection mode as function of wavelength and angle of incidence of (a) a nanocrystalline cellulose free-standing film and (b) the cuticle of the scarab beetle *Cotinis mutabilis*.

Of particular interest are the polarization properties of light reflected for unpolarized incident light with Stokes vector $\mathbf{S}_i = [1,0,0,0]^T$. In this case and according to equation (2), the reflected light is given by $\mathbf{S}_r = [1, m_{21}, m_{31}, m_{41}]^T$, i.e. the first column of $\mathbf{M}$. The elements of $\mathbf{S}_r$ can then be used in equations (3)–(5) to calculate the quantities defining the polarization properties of the reflected light as is shown in figure 4. As can be noticed at small angles of incidence, P is high in the spectral range of selective reflection and this polarized part of the reflected beam is left-handed because $e < 0$. For angles of incidence near 55° and outside the Bragg band, the reflected light is almost totally polarized $P \approx 1$, with a linear character $e \approx 0$ and s-type $\varphi \approx 90°$, which is typical of a dielectric material as in the case of beetle cuticle [20–22].

3.2. Mueller matrix and depolarization of NCC chiral films in transmission mode

Figure 5 shows the Mueller matrix measured in transmission mode at normal incidence. First, we note that $m_{41} = m_{14} > 0$ indicating that right-handed polarized light is transmitted. This is expected because as was discussed in figure 1, the films reflect left-handed polarized light. This complementarity is illustrated by including the elements m_{41} and m_{14} measured in reflection mode at angle of incidence 20°. It should be

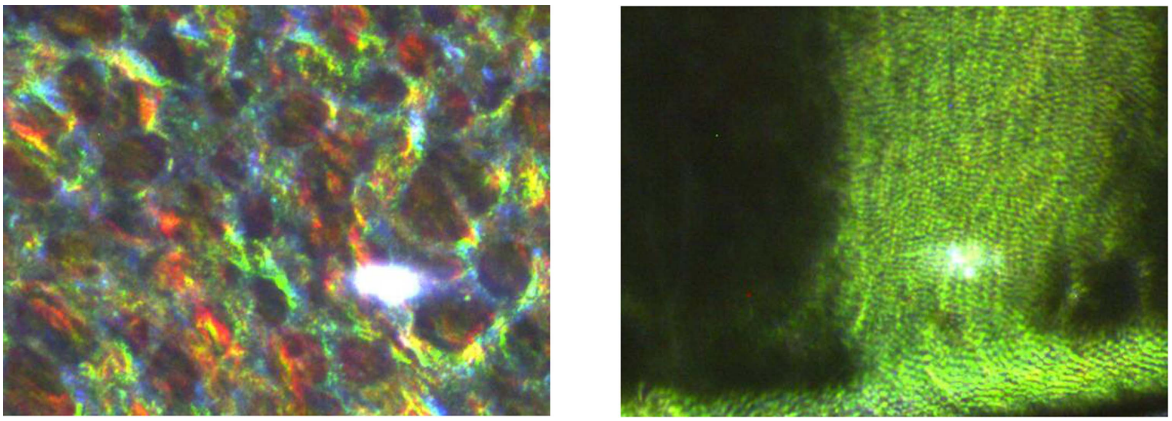

Figure 2. Optical images (4×) of a nanocrystalline cellulose film (left) and cuticle of *C. mutabilis* beetle (right). The white elliptic areas correspond to the spot of light beam probe.

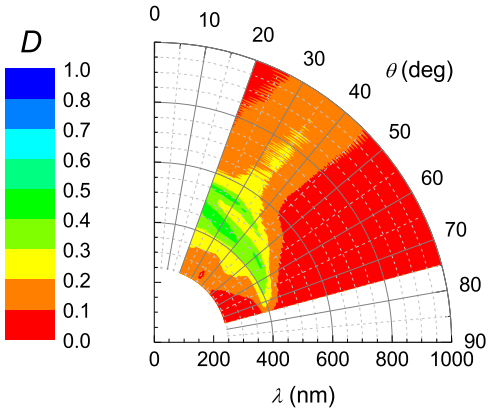

Figure 3. Depolarizance of the Mueller matrix of an NCC chiral film.

noticed that diagonal and anti-diagonal elements show appreciable values, whereas the remaining ones have values close to zero with some deviations at short wavelengths in m_{24}, m_{34}, m_{42}, and m_{43} probably due to multiple scattering.

The depolarizance of the Mueller matrix measured in transmission mode is shown in figure 6. It can be noticed that $0 \leqslant D \leqslant 0.2$ meaning that the **M** shown in figure 5 is physically meaningful. In addition, at wavelengths larger than 550 nm D is close to zero and the NCC chiral film could be considered as a non-depolarizing pure system. The increasing values of D in the band of selective reflection might be related to the multidomain texture (helicoidal axis orientation and pitch distribution) across the film. On the other hand, at wavelengths shorter than 450 nm D monotonically increases probably due to scattering.

3.3. Polarization properties of the transmitted light for unpolarized and circularly polarized incident light

It is instructive to investigate the polarization properties of light transmitted by the NCC chiral film for different polarization states of the incident beam. Using the Mueller matrix formalism, this implies straightforward calculations using equation (2). We first consider three cases of incident light: unpolarized $\mathbf{S}_{\mathrm{iU}} = [1,0,0,0]^{\mathrm{T}}$, LHCP $\mathbf{S}_{\mathrm{iLH}} = [1,0,0,-1]^{\mathrm{T}}$ and RHCP $\mathbf{S}_{\mathrm{iRH}} = [1,0,0,1]^{\mathrm{T}}$. As was noted above for $\mathbf{S}_{\mathrm{iU}}$, the Stokes vector of the transmitted beam is given by the first column of **M**, whereas for LHCP incident light it is $\mathbf{S}_t = [1 - m_{14}, m_{21} - m_{24}, m_{31} - m_{34}, m_{41} - m_{44}]^{\mathrm{T}}$ and for RHCP incident light the out coming beam has Stokes vector $\mathbf{S}_t = [1 + m_{14}, m_{21} + m_{24}, m_{31} + m_{34}, m_{41} + m_{44}]^{\mathrm{T}}$. The degree of polarization and ellipticity of the transmitted beam calculated with equations (3) and (4) for each case of incident polarization state are shown in figure 7. In figure 7(a), it can be noticed that unpolarized incident light at 515 nm emerges with a relatively high degree of polarization ($P = 0.82$) and this polarized part of the transmitted beam has a near circular right-handed character ($e = 0.85$). In figure 7(b) for LHCP incident light, the degree of polarization appreciably decreases at wavelengths in the band of selective reflection, whereas for RHCP incident light in figure 7(c) the transmitted beam is highly polarized in most of the spectral range. In both cases, the handedness of the incident beam is retained although for LHCP the ellipticity ($e = -0.55$) considerably deviates from the incident polarization state. For RHCP incident light, the ellipticity of transmitted beam is relatively high ($e = 0.84$).

Further insight into the optical response of the NCC chiral films is gained when the actual transmittance for each incident polarization state is considered. Figure 8 shows the transmittance measured in the visible range for unpolarized incident light (T_{U}), LHCP (T_{LH}), and RHCP (T_{RH}) incident light. As can be noticed, for unpolarized and LHCP incident light the band of selective reflection is evident. In contradistinction, RHCP incident light is freely transmitted. Also in figure 8 is included the polarized part of the transmittance for each case of incident light, that is, the product of the polarization degree according to equation (3) and the corresponding transmittance P_jT_j (j = U, RH, LH). Thus, the polarized and unpolarized parts are represented by the light-gray and dark-gray areas, respectively. It should be mentioned that in the ideal case of monodomain chiral nematic ordering, the baseline of T_j is expected at about 0.9 for an average refractive index of 1.54 for cellulose with a slight decrease to shorter wavelengths due to the dispersion of the refractive index. Therefore, smaller values of transmittance are indicative of light scattering. In addition, for the ideal case the minima in T_{U} and T_{LH} (at $\lambda_{\mathrm{min}} = 505$ nm) are expected to be 0.5 and 0,

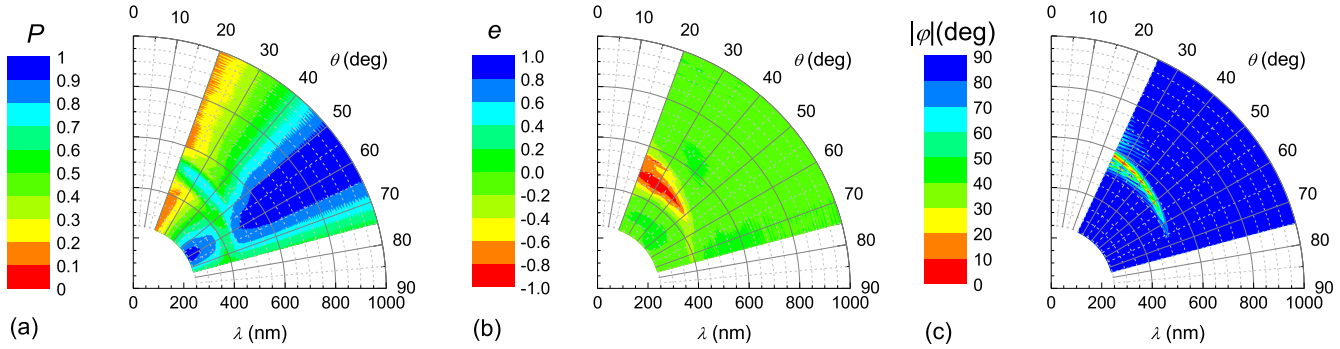

Figure 4. Polarization properties of light reflected from an NCC chiral film with unpolarized incident light: (a) degree of polarization, (b) ellipticity, and (c) azimuth.

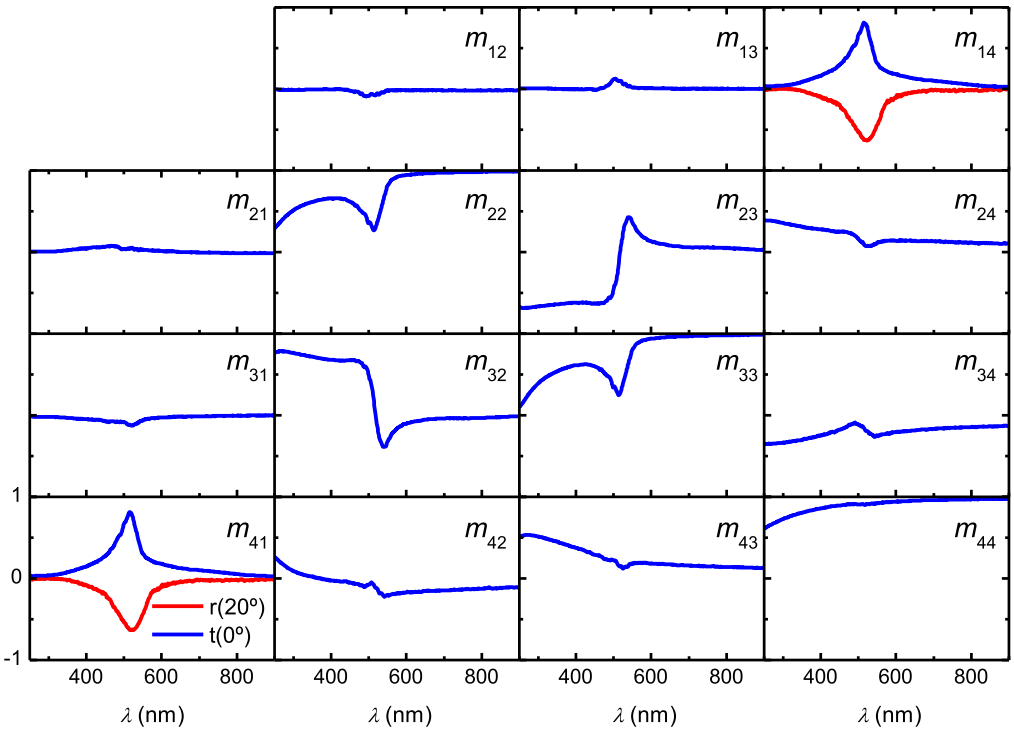

Figure 5. Transmission Mueller matrix of an NCC chiral film measured at normal incidence (0°). The elements m_{14} and m_{41} of the Mueller matrix in reflection mode (20°) are included.

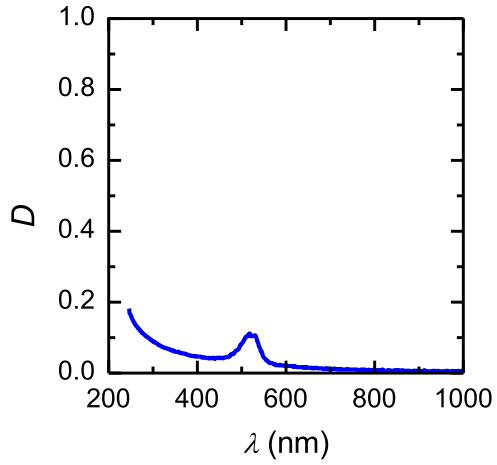

Figure 6. Depolarizance of the Mueller matrix of a chiral NCC film measured in transmission mode at normal incidence.

respectively. The larger values obtained result from the multi-domain texture. An LHCP incident light of wavelength λ_{min} will propagate through domains with pitch larger or smaller than $\Lambda = \lambda_{min}/n_{av}$ with an attenuation decreasing with the distance to λ_{min}. Also, the LHCP wave will only be partially attenuated in domains with pitch Λ if the number of turns in the helicoids is so small that the domain thickness is less than attenuation length. These two mechanisms may contribute to the non-zero value of T_{LH}. As a side result, the partial incoherent superposition of these types of contributions depolarizes the transmitted light modifying the ellipticity as well.

3.4. Polarization properties of the transmitted beam for linearly polarized incident light

Another case of interest is when the incidence is linearly polarized. As an example, we consider an incident

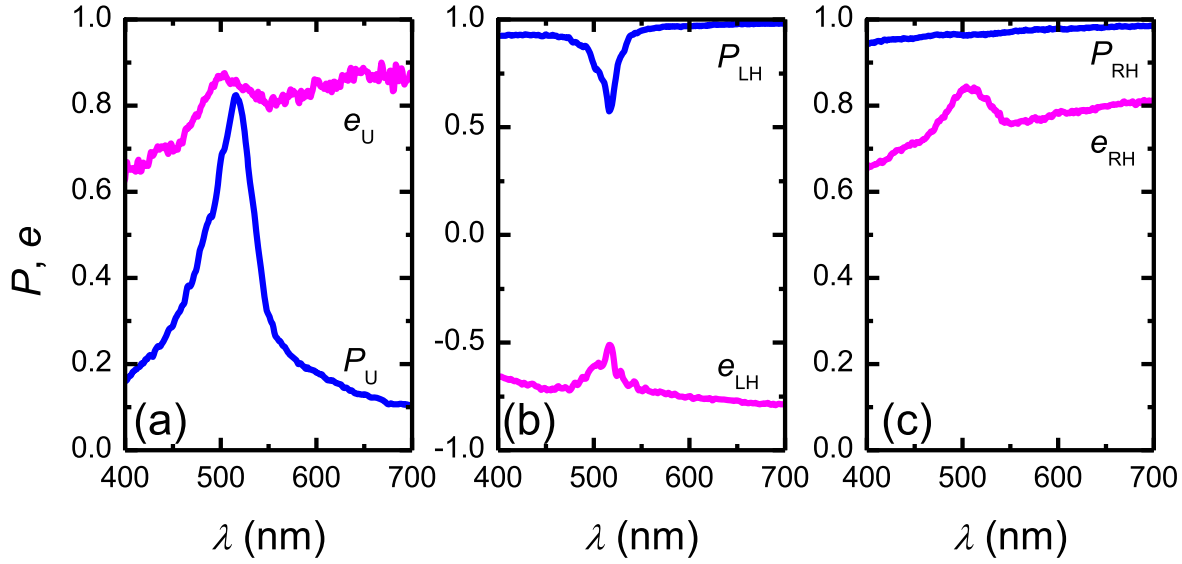

Figure 7. Degree of polarization (P) and ellipticity (e) of light transmitted through a NCC chiral film for incident light: (a) U-unpolarized, (b) LH-left-handed circularly polarized, and (c) RH-right-handed circularly polarized. Notice the different scale in (b).

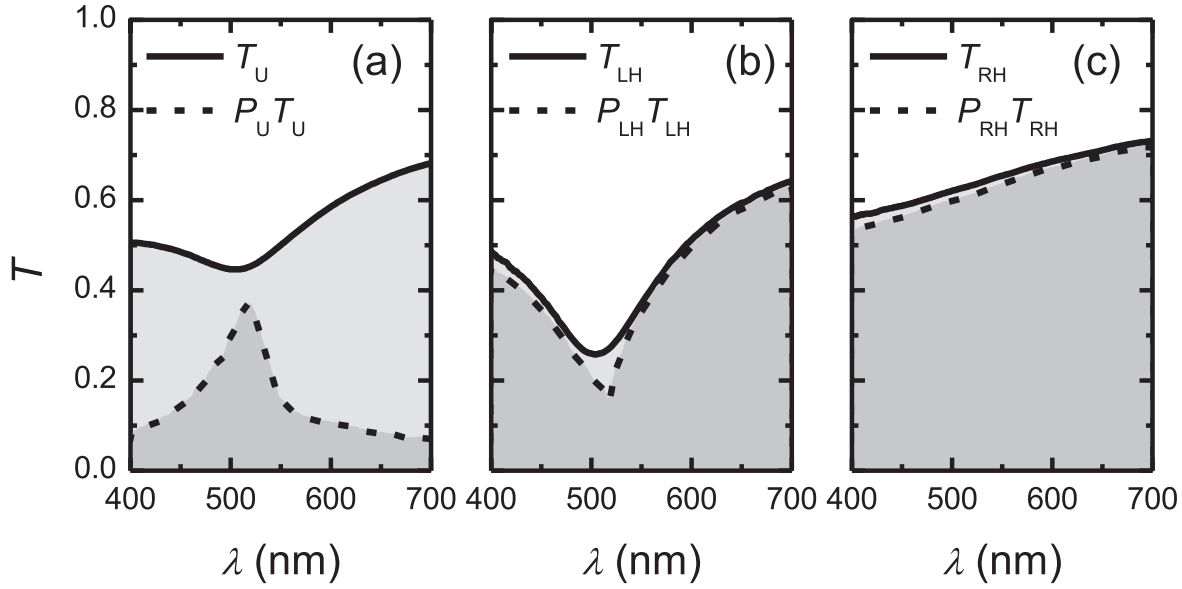

Figure 8. Transmittance of a NCC chiral film for incident light: (a) U-unpolarized, (b) LH-left-handed circularly polarized, and (c) RH-right-handed circularly polarized.

Stokes vector $\mathbf{S}_i = [1, 1, 0, 0]^T$. In this particular case, the Stokes vector of the transmitted light is $\mathbf{S}_t = [1 + m_{12}, m_{21} + m_{22}, m_{31} + m_{32}, m_{41} + m_{42}]^T$. The polarization properties of the transmitted beam calculated with equations (3)–(5) are shown in figure 9. As can be noticed in figure 9(a), the degree of polarization is relatively high with a minimum in the band of selective reflection. The polarized part of the transmitted beam is right-handed elliptically polarized in the band of selective reflection and near linearly polarized light $e \approx 0$ at larger wavelengths.

Another property of interest is the optical rotation dispersion (ORD) which results from the difference in the refractive indices for left- and right-handed circularly polarized light. In this case, ORD can be evaluated from the

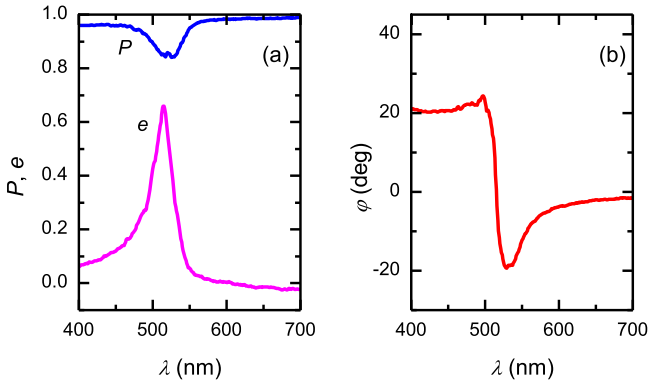

Figure 9. (a) Degree of polarization and ellipticity, and (b) azimuth angle of transmitted light for linearly polarized incident light.

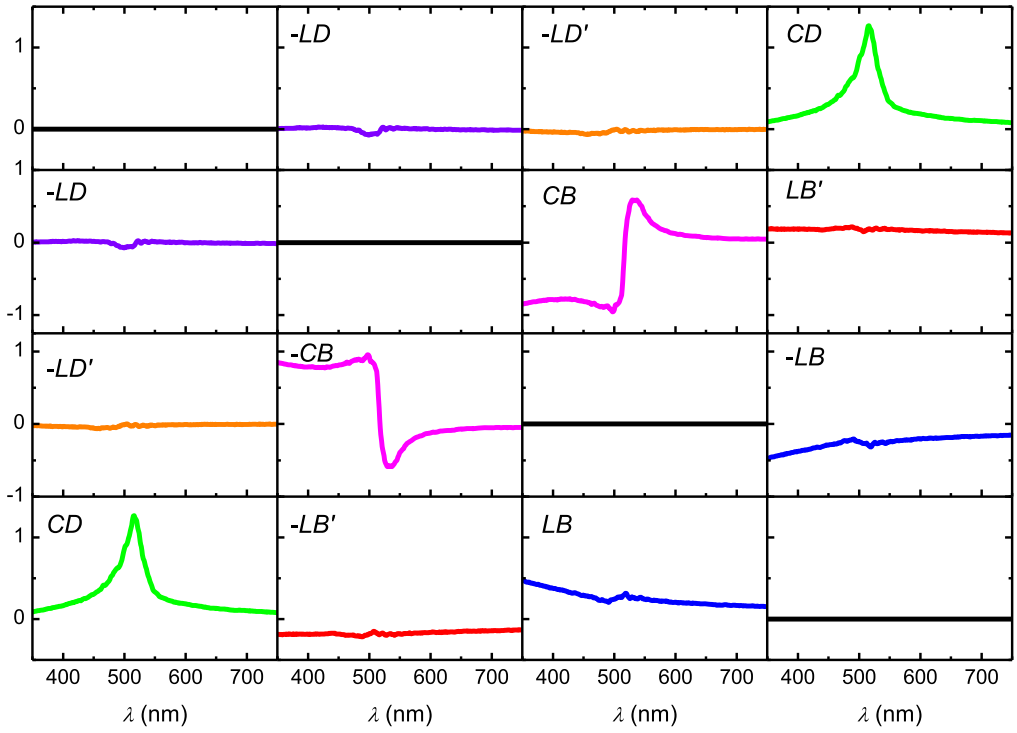

Figure 10. Matrix of elementary parameters $\mathbf{L}_m$ (equation (8)) corresponding to the transmission Mueller matrix shown in figure 5 of an NCC chiral film. The vertical scale for each row is given on the left.

azimuth of the transmitted beam shown in figure 9(b) which shows the change in azimuth for linearly polarized incident light. The maximum rotation is around $+20°$ and $-20°$ at wavelengths slightly smaller than and larger than the selective Bragg resonance wavelength. With a film thickness of 28 μm as determined by SEM we then get a maximum specific rotation of $+20/0.028 \approx +700°\,\mathrm{mm}^{-1}$ which is comparable to that found in the cuticle of the beetle *Cetonia aurata* [27]. Nevertheless, the transmitted light in the spectral band of selective reflection is right-handed ellipticaly polarized as shown in figure 9(a).

3.5. Mueller matrix differential decomposition

In chiral systems, CD is the differential absorption of LHCP and RHCP and is thus a measure of the difference between the absorption coefficients for LHCP (α_L) and RHCP (α_R) incident light. These are determined by assuming a Lambert–Beer dependence of the transmitted irradiances $I_L \sim \exp(-\alpha_L\, d)$ and $I_R \sim \exp(-\alpha_R\, d)$, where d is the sample thickness of homogenous materials with natural optical activity where LHCP and RHCP are eigenmodes of propagation [28]. In that case, for LHCP and RHCP incident light the total irradiance of the transmitted light is proportional to the first component of the Stokes vector, that is, $I_L = (1 - m_{14})$ and $I_R = (1 + m_{14})$, respectively, and CD can be quantified as,

$$\mathrm{CD} = \ln\left(\frac{1 + m_{14}}{1 - m_{14}}\right) = (\alpha_L - \alpha_R)d. \tag{7}$$

However, in anisotropic depolarizing media, equation (7) is not suitable to use for CD computation because LHCP and RHCP are not propagation eigenmodes. Recently, a differential decomposition was proposed to determine the elementary properties for homogeneous media [29, 30]. That formalism establishes that $\mathbf{M}$ and its spatial variation along the direction of wave propagation z are related as $\mathrm{d}\mathbf{M}/\mathrm{d}z = \mathbf{mM}$ where $\mathbf{m}$ is the z-independent differential matrix. Direct integration gives $\mathbf{L} = \ln\mathbf{M}$ where $\mathbf{L} = \mathbf{m}d$ being d the sample thickness. The matrix $\mathbf{L}$ is split into symmetric and asymmetric parts $\mathbf{L} = \mathbf{L}_m + \mathbf{L}_u$ where $\mathbf{L}_m = (\mathbf{L} - \mathbf{GL}^{\mathrm{T}}\mathbf{G})/2$ and $\mathbf{L}_u = (\mathbf{L} + \mathbf{GL}^{\mathrm{T}}\mathbf{G})/2$, respectively, and $\mathbf{G} = \mathrm{diag}[1, -1, -1, -1]$. Thus, $\mathbf{L}_m$ is a non-depolarizing matrix containing six elementary properties [30],

$$\mathbf{L}_m = \begin{bmatrix} 0 & -\mathrm{LD} & -\mathrm{LD}' & \mathrm{CD} \\ -\mathrm{LD} & 0 & \mathrm{CB} & \mathrm{LB}' \\ -\mathrm{LD}' & -\mathrm{CB} & 0 & -\mathrm{LB} \\ \mathrm{CD} & -\mathrm{LB}' & \mathrm{LB} & 0 \end{bmatrix}, \tag{8}$$

where LB (LD) and LB′ (LD′) are the linear birefringence (dichroism) along the x–y and $\pm 45°$ axes, CD is the circular dichroism and CB the circular birefringence. On the other hand, $\mathbf{L}_u$ is given by [30],

$$\mathbf{L}_u = \begin{bmatrix} A & \Delta p_1 & \Delta p_2 & \Delta p_3 \\ -\Delta p_1 & A - \mathrm{LDP} & \Delta p_4 & \Delta p_5 \\ -\Delta p_2 & \Delta p_4 & A - \mathrm{LDP}' & \Delta p_6 \\ -\Delta p_3 & \Delta p_5 & \Delta p_6 & A - \mathrm{CDP} \end{bmatrix}, \tag{9}$$

where LDP, LDP′, and CDP describe selective depolarization of linearly horizontal, linearly 45°, and circularly polarized light, respectively. The Δp_j elements are related to inhomogeneity in the sample or time non-reversal events [30].

Although the NCC chiral film shows a multidomain texture i.e. a non-homogeneous media, it is interesting to explore the differential decomposition of its Mueller matrix to evaluate not the intrinsic properties given in equation (8) but their equivalent effective structural parameters.

Figure 10 shows the non-depolarizing matrix $\mathbf{L}_m$ corresponding to the transmission Mueller matrix measured at normal incidence shown in figure 5. It is clear that CB and CD are the dominant elementary properties of the NCC chiral film. It should be mentioned that the off-diagonal elements in $\mathbf{L}_u$ (not shown) are $\Delta p_j \approx 0$. It is worth mentioning that $\Delta p_j = 0$ is a necessary condition for homogeneity in depolarizing media with time-reversal symmetry [30]. Introducing $\Delta\alpha = \mathrm{CD}/d$, the differential absorption per unit length attains a maximum of 45.22 mm^{-1} at wavelength 516 nm. On the other hand, diagonal elements of $\mathbf{L}_u$ have a similar wavelength dependence as the depolarizance shown in figure 6.

Current equipment routinely used to quantify CD (known as spectropolarimeters) measure only a few elements of the Mueller matrix (sometimes only one), and often anisotropic artifacts in the system affect the measurements making their interpretation difficult. Also, those equipments are limited to measure samples with low values of CD because in molecular systems the difference between the absorption coefficients α_L and α_R is very small. These limitations are overcome when the Mueller matrix approach is used in chiral films to determine the strong CD signal.

4. Conclusions

NCC chiral films were processed from bacterial cellulose. The films are iridescent and have a multidomain texture. The Mueller matrices of the films exhibit the same symmetries as those found in the cuticle of beetles having chiral structures. For unpolarized light at small angles of incidence, the films reflect partially polarized light of the left-handed type in the spectral range from 420 to 560 nm. The depolarization of NCC chiral films in reflection mode is larger compared to that observed in beetle´s cuticle. For unpolarized light at normal incidence, the films transmit right-handed polarized light. In the band of selective reflection, the depolarization depends on the state of polarization of the incident light but right-handed polarized light is not largely affected. The depolarization increases at short wavelengths probably due to multiple scattering. For longer wavelengths, the depolarization is almost zero. Large values of structural circular birefringence and dichroism were determined using a differential decomposition of the transmission Mueller matrix at normal incidence.

Acknowledgments

The Knut and Alice Wallenberg foundation, the Swedish Research Council, Carl Tryggers foundation and the Swedish Government Strategic Research Area in Materials Science on Functional Materials at Linköping University (Faculty Grant SFO-Mat-LiU # 2009-00971) are acknowledged for financial support. Brazilian agencies FAPESP and CNPq are acknowledged for financial support. Moliria Vieira dos Santos acknowledges FAPESP for a doctoral fellowship (grants #2014/12424-2).

ORCID iDs

Arturo Mendoza-Galván https://orcid.org/0000-0003-2418-5436
Eloy Muñoz-Pineda https://orcid.org/0000-0003-3807-3312
Sidney J L Ribeiro https://orcid.org/0000-0003-3286-9440
Moliria V Santos https://orcid.org/0000-0003-0569-2424
Kenneth Järrendahl https://orcid.org/0000-0003-2749-8008
Hans Arwin https://orcid.org/0000-0001-9229-2028

References

[1] Bouligand Y 1972 Twisted fibrous arrangements in biological materials and cholesteric mesophases *Tissue Cell* **4** 189–217
[2] Giraud-Guille M M, Besseau L and Martin R 2003 Liquid crystalline assemblies of collagen in bone and in vitro systems *J. Biomech.* **36** 1571–9
[3] Vignolini S, Moyroud E, Glover B J and Steiner U 2013 Analysing photonic structures in plants *J. R. Soc. Interface* **10** 20130394
[4] Lenau T and Barfoed M 2008 Colours and metallic sheen in beetle shells—a biomimetic search for material structuring principles causing light interference *Adv. Eng. Mater.* **10** 299–314
[5] Faryad M and Lakhtakia A 2014 The circular Bragg phenomenon *Adv. Opt. Photon.* **6** 225–92
[6] Revol J F, Bradford H, Giasson J, Marchessault R H and Gray D G 1992 Helicoidal self-ordering of cellulose microfibrils in aqueous suspension *Int. J. Biol. Macromol.* **14** 170–2
[7] Beck S, Bouchard J and Berry R 2011 Controlling the reflection wavelength of iridescent solid films of nanocrystalline cellulose *Biomacromolecules* **12** 167–72
[8] Kelly J A, Giese M, Shopsowitz K E, Hamad W Y and MacLachlan M J 2014 The development of chiral nematic mesoporous materials *Acc. Chem. Res.* **47** 1088–96
[9] Lagerwall J P F, Schütz C, Salajkova M, Noh J H, Park J H, Scalia G and Bergström L 2014 Cellulose nanocrystal-based materials: from liquid crystal self-assembly and glass formation to multifunctional thin films *NPG Asia Mater.* **6** 1–12
[10] Park J H, Noh J H, Schütz C, Salazar-Alvarez G, Scalia G, Bergström L and Lagerwall J P F 2014 Macroscopic control of helix orientation in films dried from cholesteric liquid-crystalline cellulose nanocrystal suspensions *Chem. Phys. Chem.* **15** 1477–84
[11] Mu X and Gray D G 2014 Formation of chiral nematic films from cellulose nanocrystal suspensions is a two-stage process *Langmuir* **30** 9256–60

[12] Dumanli G, van der Kooij H M, Kamita G, Reisner E, Baumberg J J, Steiner U and Vignolini S 2014 Digital color in cellulose nanocrystal films *ACS Appl. Mater. Interfaces* **6** 12302–6
[13] Dumanli A G, Kamita G, Landman J, van der Kooij H, Glover B J, Baumberg J J, Steiner U and Vignolini S 2014 Controlled, bio-inspired self-assembly of cellulose-based chiral reflectors *Adv. Opt. Mater.* **2** 646–50
[14] Querejeta-Fernández A, Kopera B, Prado K S, Klinkova A, Methot M, Chauve G, Bouchard J, Helmy A S and Kumacheva E 2015 Circular dichroism of chiral nematic films of cellulose nanocrystals loaded with plasmonic nanoparticles *ACS Nano* **9** 10377–85
[15] Giese M, Blusch L K, Khan M K and MacLachlan M J 2015 Functional materials from cellulose-derived liquid-crystal templates *Angew. Chem., Int. Ed.* **54** 2888–910
[16] Santos M V, Tercjak A, Gutierrez J, Barud H, Napolia M, Nalina M and Ribeiro S L J 2017 Optical sensor platform based on cellulose nanocrystals (CNC)-4-(hexyloxy)-4-biphenylcarbonitrile (HOBC) bi-phase nematic liquid crystal composite films *Carbohydr. Polym.* **168** 346–55
[17] Arwin H, Magnusson R, Landin J and Järrendahl K 2012 Chirality-induced polarization effects in the cuticle of scarab beetles: 100 years after Michelson *Phil. Mag.* **92** 1583–99
[18] Arwin H, Berlind T, Johs B and Järrendahl K 2013 Cuticle structure of scarab beetles analyzed by regression analysis of Mueller-matrix ellipsometric data *Opt. Express* **21** 22645–56
[19] Arwin H, Fernández del Río L and Järrendahl K 2014 Comparison and analysis of Mueller-matrix spectra from exoskeletons of blue, green and red Cetonia aurata *Thin Solid Films* **571** 739–43
[20] Muñoz-Pineda E, Järrendahl K, Arwin H and Mendoza-Galván A 2014 Symmetries and relationships between elements of the Mueller matrix spectra of the cuticle of the beetle Cotinis mutabilis *Thin Solid Films* **571** 660–5
[21] Mendoza-Galván A, Muñoz-Pineda E, Järrendahl K and Arwin H 2014 Evidence for a dispersion relation of optical modes in the cuticle of the scarab beetle Cotinis mutabilis *Opt. Mater. Express* **4** 2484–96
[22] Fernández del Río L, Arwin H and Järrendahl K 2016 Polarizing properties and structure of the cuticle of scarab beetles from the Chrysina genus *Phys. Rev.* E **94** 012409
[23] Goldstein D H 2010 *Polarized Light* (Boca Raton, FL: CRC Press)
[24] Takezoe H, Ouchi Y, Hara M, Fukuda A and Kuze E 1983 Experimental studies on reflection spectra in monodomain cholesteric liquid crystal cells: total reflection, subsidiary oscillation and its beat or swell structure *Japan. J. Appl. Phys.* **22** 1080–91
[25] Seferis J C 1999 Refractive index of polymers *Polymer Handbook* ed J Brandrup *et al* 4th edn (New York: Wiley)
[26] Gil J J 2007 Polarimetric characterization of light and media *Eur. Phys. J. Appl. Phys.* **40** 1–47
[27] Arwin H, Mendoza-Galván A, Magnusson R, Andersson A, Landin J, Järrendahl K, Garcia-Caurel E and Ossikovski R 2016 Structural circular birefringence and dichroism quantified by differential decomposition of spectroscopic transmission Mueller matrices from Cetonia aurata *Opt. Lett.* **41** 3293–6
[28] Arteaga O 2016 Natural optical activity versus circular Bragg reflection studied by Mueller matrix ellipsometry *Thin Solid Films* **617** 14–9
[29] Ossikovski R 2011 Differential matrix formalism for depolarizing anisotropic media *Opt. Lett.* **36** 2330–2
[30] Arteaga O and Kahr B 2013 Characterization of homogenous depolarizing media based on Mueller matrix differential decomposition *Opt. Lett.* **38** 1134–6